FLOW REGIME IDENTIFICATION OF HORIZONTAL TWO PHASE REFRIGERANT R-134a FLOW USING NEURAL NETWORKS (POSTPRINT)

Paul J. Kreitzer

UES Inc.

Michael Hanchak

University of Dayton Research Institute

Larry Byrd

Mechanical and Thermal Systems Branch
Power and Control Division

NOVEMBER 2013

STINFO COPY

AIR FORCE RESEARCH LABORATORY
AEROSPACE SYSTEMS DIRECTORATE
WRIGHT-PATTERSON AIR FORCE BASE, OH 45433-7542
AIR FORCE MATERIEL COMMAND
UNITED STATES AIR FORCE

NOTICE AND SIGNATURE PAGE

*//Signature//

TRAVIS E. MICHALAK
Program Manager
Mechanical and Thermal Systems Branch
Power and Control Division

//Signature//

THOMAS L. REITZ, Technical Advisor
Mechanical and Thermal Systems Branch
Power and Control Division
Aerospace Systems Directorate

//Signature//

JOHN G. NAIRUS, Chief Engineer
Power and Control Division
Aerospace Systems Directorate

REPORT DOCUMENTATION PAGE		*Form Approved* *OMB No. 0704-0188*

The public reporting burden for this collection of information is estimated to average 1 hour per response, including the time for reviewing instructions, searching existing data sources, searching existing data sources, gathering and maintaining the data needed, and completing and reviewing the collection of information. Send comments regarding this burden estimate or any other aspect of this collection of information, including suggestions for reducing this burden, to Department of Defense, Washington Headquarters Services, Directorate for Information Operations and Reports (0704-0188), 1215 Jefferson Davis Highway, Suite 1204, Arlington, VA 22202-4302. Respondents should be aware that notwithstanding any other provision of law, no person shall be subject to any penalty for failing to comply with a collection of information if it does not display a currently valid OMB control number. **PLEASE DO NOT RETURN YOUR FORM TO THE ABOVE ADDRESS.**

1. REPORT DATE *(DD-MM-YY)* November 2013	2. REPORT TYPE Conference Paper Postprint	3. DATES COVERED *(From - To)* 01 April 2012 – 08 April 2013	
4. TITLE AND SUBTITLE FLOW REGIME IDENTIFICATION OF HORIZONTAL TWO PHASE REFRIGERANT R-134a FLOW USING NEURAL NETWORKS (POSTPRINT)			5a. CONTRACT NUMBER In-house
			5b. GRANT NUMBER
			5c. PROGRAM ELEMENT NUMBER 62203F
6. AUTHOR(S) Paul J. Kreitzer (UES Inc.) Michael Hanchak (University of Dayton Research Institute) Larry Byrd (AFRL/RQQM)			5d. PROJECT NUMBER 3145
			5e. TASK NUMBER N/A
			5f. WORK UNIT NUMBER Q0LA
7. PERFORMING ORGANIZATION NAME(S) AND ADDRESS(ES) UES Inc. 4401 Dayton-Xenia Road Dayton, OH 45432 -- University of Dayton Research Institute 300 College Park Dayton, OH 45469	Mechanical and Thermal Systems Branch (AFRL/RQQM) Power and Control Division Air Force Research Laboratory Aerospace Systems Directorate Wright-Patterson Air Force Base, OH 45433-7542 Air Force Materiel Command, United States Air Force		8. PERFORMING ORGANIZATION REPORT NUMBER AFRL-RQ-WP-TP-2014-0132
9. SPONSORING/MONITORING AGENCY NAME(S) AND ADDRESS(ES) Air Force Research Laboratory Aerospace Systems Directorate Wright-Patterson Air Force Base, OH 45433-7542 Air Force Materiel Command United States Air Force			10. SPONSORING/MONITORING AGENCY ACRONYM(S) AFRL/RQQM
			11. SPONSORING/MONITORING AGENCY REPORT NUMBER(S) AFRL-RQ-WP-TP-2014-0132

12. DISTRIBUTION/AVAILABILITY STATEMENT
Approved for public release; distribution unlimited.

13. SUPPLEMENTARY NOTES
PA Case Number: 88ABW-2013-1704; Clearance Date: 08 Apr 2013. The conference paper was presented at the ASME 2013 International Mechanical Engineering Congress and Exposition, held in San Diego, California, from November 15 through 21, 2013 and was published in the ASME proceedings of the conference, Paper Number IMECE2013-62510.

The U.S. Government is joint author of the work and has the right to use, modify, reproduce, release, perform, display, or disclose the work.

14. ABSTRACT
Flow regime Identification is an integral aspect of modeling two phase flows as most pressure drop and heat transfer correlations rely on a priori knowledge of the flow regime for accurate system predictions. In the current research, two phase R-134a flow is studied in a 7mm adiabatic horizontal tube over a mass flux range of 100-400 kg/m2s between 550-750 kPa. Electric Capacitance Tomography results for 196 test points were analyzed using statistical methods and neural networks.

This data provided repeatable normalized permittivity ratio signatures based on the flow distributions. The first four temporal moments from the mean scaled permittivity data were utilized as input variables. Results showed that only 80 percent of flow regimes could be correctly identified using seven flow regime classifications. However reducing to five more commonly used regimes resulted in an improvement to 99 percent of the flow regimes correctly identified. Both methods of neural network training resulted in errors that were off by mostly one flow regime classification. Further analysis shows that transition cases can oscillate between two separate flow regimes at the same time.

15. SUBJECT TERMS thin film evaporation, modeling, Retarded Van Der Waals Interaction, heat transfer

16. SECURITY CLASSIFICATION OF:			17. LIMITATION OF ABSTRACT: SAR	18. NUMBER OF PAGES 16	19a. NAME OF RESPONSIBLE PERSON (Monitor) Travis E. Michalak
a. REPORT Unclassified	b. ABSTRACT Unclassified	c. THIS PAGE Unclassified			19b. TELEPHONE NUMBER *(Include Area Code)* N/A

Standard Form 298 (Rev. 8-98)
Prescribed by ANSI Std. Z39-18

IMECE2013-62510

FLOW REGIME IDENTIFICATION OF HORIZONTAL TWO PHASE REFRIGERANT R-134a FLOW USING NEURAL NETWORKS[1]

Paul J. Kreitzer
Aerospace Power & Propulsion Technologies Division
UES Inc.
Dayton, Ohio 45432
Paul.kreitzer.ctr@wpafb.af.mil

Michael Hanchak
Modeling and Simulation Group
University of Dayton Research Institute
Dayton, Ohio 45469
Michael.hanchak.ctr@wpafb.af.mil

Larry Byrd
Propulsion Directorate, AFRL/RZPS
U.S. Air Force Research Laboratory
Wright Patterson Air Force Base, Ohio 45433
Larry.byrd@wpafb.af.mil

ABSTRACT

Flow regime Identification is an integral aspect of modeling two phase flows as most pressure drop and heat transfer correlations rely on a priori knowledge of the flow regime for accurate system predictions. In the current research, two phase R-134a flow is studied in a 7mm adiabatic horizontal tube over a mass flux range of 100-400 kg/m^2s between 550-750 kPa. Electric Capacitance Tomography results for 196 test points were analyzed using statistical methods and neural networks. This data provided repeatable normalized permittivity ratio signatures based on the flow distributions. The first four temporal moments from the mean scaled permittivity data were utilized as input variables. Results showed that only 80 percent of flow regimes could be correctly identified using seven flow regime classifications. However reducing to five more commonly used regimes resulted in an improvement to 99 percent of the flow regimes correctly identified. Both methods of neural network training resulted in errors that were off by mostly one flow regime classification. Further analysis shows that transition cases can oscillate between two separate flow regimes at the same time.

NOMENCLATURE

A	=	Input matrix
$\alpha(t)$	=	void fraction
b	=	Target vector
D	=	Channel diameter (m)
D_H	=	Hydraulic diameter (m)
ε^*	=	Normalized permittivity ratio
$\overline{\varepsilon^*}(t)$	=	Spatial mean for ε_*
G	=	Total mass flux (kg/m^2s)
L	=	Channel length (m)
n	=	Number of electrodes
N	=	Number of bins
x	=	coefficient vector

Subscripts

f	=	liquid
v	=	vapor

Acronyms

ECT	=	Electrical capacitance tomography
fps	=	Frames per second
ID	=	Inner diameter
LBP	=	Linear back projection
lpm	=	liter per minute
OC	=	Observation channel
PDF	=	Probability density function

INTRODUCTION

Flow regime identification is necessary for accurate prediction and modeling of two-phase flow systems. Classifications descriptions focus on tracking the evolution of liquid and vapor distributions within the channel over time.

---

[1] This manuscript was prepared, in part, by a U.S. Government employee on official time, is not subject to copyright and is in the public domain.

Body forces acting on the two-phase mixture influence phase distributions as well as the shape of the interface between phases. Horizontal channel flow has three major classifications, bubbly, intermittent and annular flows; where intermittent flow is further divided into plug, slug and stratified wavy flows [1-3].

Most correlations for heat transfer coefficient or pressure drop require a priori knowledge of the flow regime based on steady state operation of the channel. Measurement and detection of changes in flow regime improve thermal management system modeling efforts. Historically, identification and classification of horizontal two-phase flow regimes relies on human interpretation of measured signals. Variations in flow regime labels and identification definitions results in discrepancies when comparing results from one research effort to another. Rosa et al. [4] used six identification groups instead of the traditional four to capture transitions better when observing vertical two-phase flows. Departures like these make direct comparison between different techniques difficult.

Classification techniques include wavelet transformations, fractal analysis, pressure signature tracking, ECT signature analysis, and neural networks [5-9]. Each technique has advantages and disadvantages. Electrical Capacitance Tomography (ECT) is a non-invasive impedance measurement method that produces mean normalized permittivity ratio, $\overline{\varepsilon^*}$, values that are directly linked to void fraction correlations. This paper utilizes ECT data as input parameters for neural networks.

Hu et al. [10] studied the behavior of two-phase gas/solid vertical flows using electrostatic techniques. Raw electrostatic signals showed random fluctuations with only minor differences in amplitude. The signals were analyzed using three different techniques, short-term average energy, Mel frequency cepstrum coefficient, and cepstrum. Each of the individual signal analysis techniques resulted in marginal performance from the neural network (67% to 89% recognition rate), however, combining the three techniques increased the accuracy to 97%.

Mi et al. [11] points out that most flow pattern maps depend on superficial velocities, however in most systems these parameters are often impossible to measure directly. As a result they studied void fraction measurements based on impedance measurements. However, they needed to remove system noise and therefore used simulated impedance signals as input data for their neural network. Two different neural network techniques were used to sort the data, a supervised neural network and a self-organizing neural network. Results showed good agreement between the techniques. Comparisons with existing empirical data in Mishima and Ishii [12] showed that neural networks indicate proper flow regime classifications.

Rosa et al. [4] investigated the use of neural networks in vertical liquid vapor flows. Their work compared results obtained based on prior identification via a human specialist with a clustering algorithm that automatically binned the data based only on data signals. The results from this study suggest that the use of a human specialist to visually classify flow regime labels before training in the neural network improved network accuracy by 40%.

Ghosh et al. [13] compared data collected with a ring electrode configuration with that of a parallel wire configuration for counter current vertical pipe flow. The results showed that data collected with the ring probe failed to capture the hydrodynamic properties of the two phase air water system. However, the data collected with the parallel wire probe was sufficient to predict flow regimes. Data analysis looked into statistical parameters based on the parallel wire probe signals. It was found that the mean and standard deviation were most helpful, while the skewness and kurtosis did not capture changes in flow conditions.

The research presented in this paper focuses on ECT signal analysis of horizontal two-phase refrigerant flows. Neural networks are applied, varying input parameters and algorithm control of the network, to investigate the influence on flow regime identification. This paper consists of a brief experimental description, with sections focusing on visualization results and ECT signal interpretation. The automatic flow regime identification using neural networks is then explained. Finally, results are then presented and discussed followed by concluding statements.

EXPERIMENTAL APPARATUS

A schematic for the experimental setup is provided in Figure 1. The apparatus for the current work consists of two separate loops, 1) R-134a test loop and 2) Water Cooling loop. A pumped refrigeration loop is utilized to ensure the purity of the refrigerant by avoiding the use of lubrication oils. Single phase liquid refrigerant enters a minichannel heat exchanger which is heated by two aluminum nitride heaters resulting in two phase flow. The heat exchanger has 40 rectangular sections with a hydraulic diameter, D_H, of 1.4mm. Exiting two phase flows mix in an exit plenum before entering a clear, fused quartz, D_H = 7mm ID observation channel with downstream length of 300 diameters.
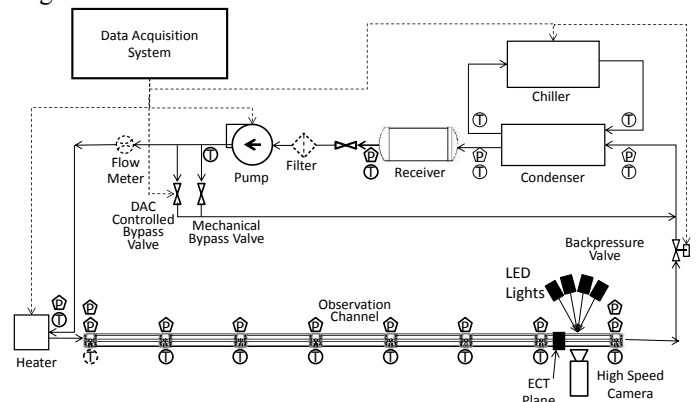

Figure 1. Schematic of two phase flow system.

The observation channel is equipped with thermocouple and pressure transducer measurements at 0.35m increments. Transparent channel sections allow for real time observation

and recording using a Phantom V4.2 high speed video camera. A non-intrusive electrical capacitance tomography section is wrapped around the channel and used to measure the liquid-vapor distribution traveling through the channel. Both high speed video and ECT measurements are taken between an L/D of 280 and 300 to ensure that the two phase flow is fully developed. Testing was performed with refrigerant saturation conditions set for room temperature of 20 °C. Minimal deviations from this temperature during testing provide grounds for an adiabatic assumption.

A condenser removes the heat from the two-phase refrigerant, returning it to a single-phase liquid flow entering the receiver. Uncertainty measurements are tracked for all equipment in the system. Type T thermocouples were calibrated to ±0.1 °C using a Fluke constant temperature bath. Omega PX-409 pressure transducers were calibrated to ± 0.1% full scale using a Heise handheld pressure calibrator between 35 and 760 kPa. Finally, a McMillan flow meter was calibrated to 0.6% full scale using Air Force Standard F242007 for mass flux from 0-500 kg/m^{2}s. The condenser is connected to a NESLAB RTE 17 constant temperature bath with temperature stability of ± 0.01 °C.

Non-invasive measurements are accomplished using a high-speed video camera and the ECT measurement system. A phantom V4.2 high-speed video camera provides the ability to analyze the two-phase flow allowing for a subjective classification technique. The ECT system is comprised of a clamp on sensor and an electronics box that handles control, data acquisition and data reduction for the sensor. The sensor is approximately 150 mm long and consists of grounded entrance and exit regions on either side of eight 51mm long electrodes positioned axially along the tube at equal angular spacing, see Figure 2. The electronics box contains a power supply and software to sequentially apply a voltage to one of the eight electrodes and measure the resulting voltage at each of the remaining electrodes.
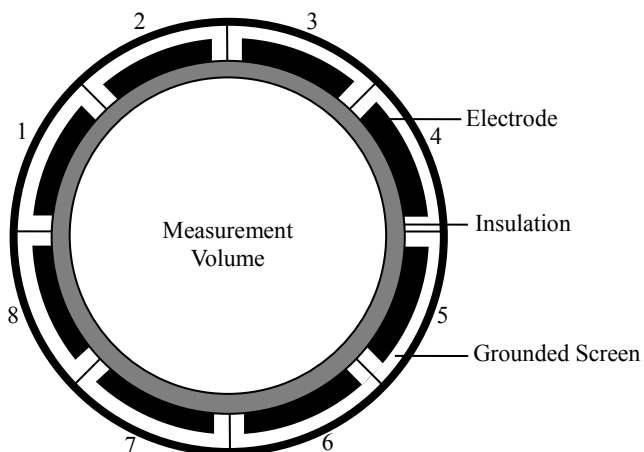

Figure 2. ECT Sensor with eight electrodes.

A single tomogram is generated by taking a series of 28 individual measurements in quick succession (n(n-1)/2 = 28).

Tomograms are graphical representations of numerically calculated normalized permittivity ratio values that represent the liquid-vapor distribution. The normalized permittivity ratio is given as $\varepsilon_*(\tilde{x}, t) = \left(\varepsilon(\tilde{x}, t) - \varepsilon_g\right)/\left(\varepsilon_f - \varepsilon_g\right)$ where ε_f and ε_g are the permittivities of the liquid and gas phases. $\tilde{x}$ represents the spatial variables, x, y and t is time. This process assigns a value of zero for complete vapor and a value of 1 for complete liquid. Tomograms values are calculated using a linear back projection reconstruction algorithm that creates a 32x32-pixel map. Each pixel value, or sub-volume, is a volumetric representation proportional to the normalized permittivity ratio within the measurement volume of the sensor.

The software accounts for the presence of the quartz tube by taking single phase reference measurements with vapor only or liquid only. Because of the length of the electrodes it is important to note that each measurement is proportional to a volume and not a cross section. Thus, the tomogram will have regions that are assigned values of permittivity between zero and one because the sub-volume associated with a given pixel can consist of both liquid and vapor at the time of the measurement.

The volumetric representation and the time to take the measurements limits the resolution of the sensor. For example, at the fastest setting, it takes approximately 17ms to take a frame with a millisecond delay between frames. In this time, a feature that is moving at approximately 2.8m/s would pass from the entrance to the exit of the sensor and the recorded permittivity would be an average during that time. This is not a problem for stratified or annular flows that have stable phase distributions but could cause problems during intermittent flows. What is being used for flow regime identification is the spatial mean normalized permittivity ratio, or liquid fraction, $\overline{\varepsilon^*}(t) = \frac{1}{A} \iint \varepsilon_*(\tilde{x}, t) \, dA$. For the present paper the data represents the values averaged over three frames taken at approximately 20ms each to provide smoothing. The spatial average is taken over the 812 pixel values inside of the tube. As mentioned previously, the value for $\varepsilon_*(\tilde{x}, t)$ is averaged over the length of the sensor thus it is averaged over time and volume and not an instantaneous value at a given cross section. A complete description of the ECT measurement process can be found in Kreitzer, 2012[14].

EXPERIMENTAL ANALYSIS

Two phase flow regimes

Typical horizontal two phase flow studies are divided into five regimes, bubbly, plug, slug, stratified wavy, and annular flows. High speed video analysis demonstrates the liquid vapor distributions for each flow regime as seen in Figure 3. Each test point described in this paper is accompanied by high speed video for visual verification of the measured void fractions using ECT signals. Brief descriptions of each flow regime follows.

Bubbly flow is the first flow regime beyond that of single phase liquid flows. Small discrete bubbles are formed and move along the top of the channel. Channel size dictates that

gravitational and buoyancy forces dominate. Bubble sizes vary, but are typically smaller than the channel diameter.

Plug flow occurs when adjacent bubbles coalesce into small Taylor bubbles, separated by liquid plugs. The bubble diameter remains smaller than the channel diameter and the length extends to several channel diameters. Bubbles often consist of a larger rounded front section followed by a smaller slightly elongated tail section.
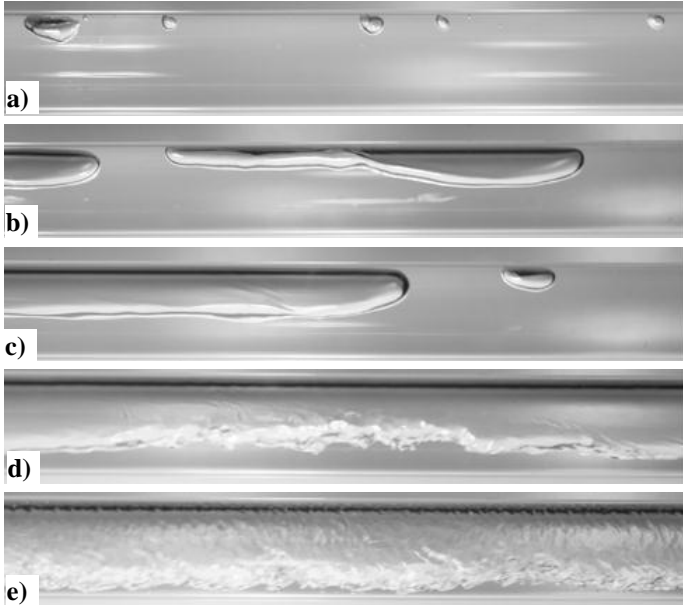

Figure 3. High speed video images depicting: a) Bubbly, b) Plug, c) Slug, d) Stratified wavy, and e) Annular horizontal channel flows.

Slug flow is a continuation of plug flow where the Taylor bubbles continue to grow in length and can approach 50-80 times the channel diameter. Bubble shapes start to form a consistent bullet shape with a rounded nose and blunt tail. The diameter of the vapor bubbles starts to approach the channel diameter. Liquid slugs separate vapor bubbles and can entrain small dispersed bubbles.

Stratified wavy flow occurs with higher vapor velocities. The clearly defined liquid slugs are no longer present and a continuous vapor layer occurs along the top of the channel. Instabilities remain along the interface between the liquid and vapor sections that can be observed as waves propagating down the length of the channel. These waves will not reach the top of the channel; however will result in a wetting of the walls of the channel leaving behind thin films.

Annular flow occurs when the vapor velocity increases further and a ring of liquid flow surrounds a central core of vapor flow. Due to channel size, a thicker layer will remain along the bottom of the channel. Small waves still exist resulting in a rippled view along all sides of the channel.

ECT Signal Analysis

The normalized permittivity ratio provides a non-intrusive method for tracking the distribution of liquid and vapor within the channel over time. The mean normalized permittivity ratio represents the liquid fraction in the sensor volume. From these measurements, the void fraction, α can be calculated as $\alpha(t) = 1 - \bar{\varepsilon}^*t)$ as described in Kreitzer[14]. Each flow regime results in a unique ECT permittivity pattern that can be used in differentiating between flow regimes. Figure 4 reveals how the normalized permittivity ratio values show a clearly identifiable trend between flow regimes. These plots provide a method for observing the void fraction, by looking at the mean of the normalized permittivity ratio. Similarly, the liquid vapor oscillations can be identified by watching the peak and valley values. Figure 5 converts the information presented in Figure 4 into Probability Density Functions (PDFs) showing the distribution of normalized permittivity ratio values for each classification; all 196 cases are plotted in Figure 8.

This section explains typical measurements for $\bar{\varepsilon}^*(t)$ and the subsequently formed PDF for each of the five main flow regimes observed during two phase flow in a horizontal channel.

Bubbly flow presents a relatively smooth curve with values of $\bar{\varepsilon}^*$ ranging between 0.85-1. Bubbly flow is dominated by small discrete bubbles that are much smaller than the measurement volume. Thus detection of individual bubbles is nearly impossible. However, signal fluctuations can occur when multiple bubbles pass through at the same time. Taking the PDF of bubbly flow shows single peak near the upper end of the permittivity range indicating that most of the flow is liquid with a small amount of vapor present.

Plug Flow demonstrates growth of a semi-periodic fluctuation in $\bar{\varepsilon}^*$ with values ranging from 0.7-0.95. This fluctuation is expected as the growing vapor bubbles coalesce and form Taylor bubbles separated by liquid plugs during flow. Observations of the PDF show two distinct peaks indicating the bounds of the alternating liquid and vapor phases.

Slug flow permittivity values range from 0.3-0.95. The large fluctuations are explained by the periodic passage of long vapor bubbles and short liquid slug regions with almost complete liquid fill and occasional bubbles. Looking at the PDF curve shows that the two peaks shows further separation showing an increase in void fraction and greater dependence on the oscillatory behavior of the flow.

Stratified wavy flow shows a decrease in $\bar{\varepsilon}^*$ between 0.2-0.4. The signal appears to be noisier due to the passage of randomly sized waves through the channel at different intervals. The PDF curve shows a single, wide spike with a slightly longer tail on the right hand side showing that the periodic passage of vapor pockets has dissipated leaving constant vapor presence along the top half of the channel. The extended tail on the right hand side of the PDF curve indicates that occasional waves of measureable amplitude are present.

Annular flow signals smooth out greatly as the waves from stratified wavy flows subside. $\bar{\varepsilon}^*$ values range from 0.1-0.25.

Approved for public release; distribution unlimited.

The PDF curve shows a sharper and narrower peak with a smaller $\overline{\varepsilon^*}$ value indicating mostly vapor presence in the channel.

Table 1 presents an average value for each of the first four moments of the $\overline{\varepsilon^*}$ curves for all 196 test cases. Variance values provide an indication of the amplitude of the fluctuations of the ECT data and indicate a maximum value associated with slug flow, which is to be expected. Skewness values tend to increase with changes in flow regime and kurtosis values show less of a definitive trend. This data is used in the next section as input data for the neural network.
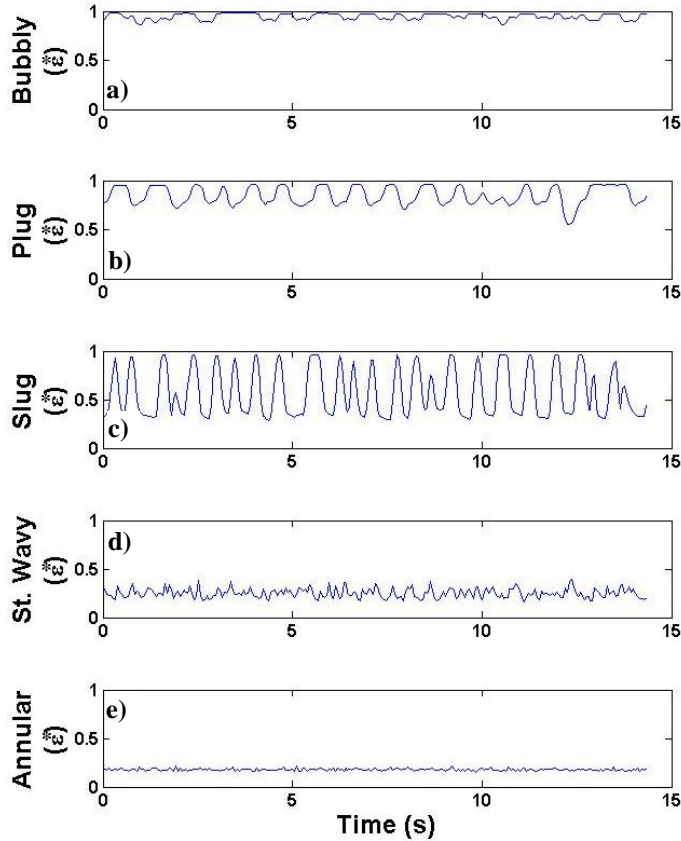
Figure 4. Selected $\overline{\varepsilon^*}$ data plotted for each flow regime: a) Bubbly, b) Plug, c) Slug, d) Stratified wavy, and e) Annular flows.

Table 1. First four moments of $\overline{\varepsilon^*}$ curves corresponding to 196 test cases over five categories.

Flow Regime	Mean	Variance	Skewness	Kurtosis
Bubbly	0.9443	0.0010	-0.4446	2.0435
Plug	0.8459	0.0084	-0.2808	2.4916
Slug	0.5671	0.0589	0.4865	1.6134
St. Wavy	0.2509	0.0024	0.4697	2.7235
Annular	0.1773	0.0001	0.7320	3.6014

AUTOMATIC FLOW REGIME IDENTIFICATION

The raw ECT data for a given case is represented by a 256-row and 812-column matrix of values between zero and one, inclusive. Each row of the matrix or tomogram frame represents a volumetric slice in time and consists of 812 pixels
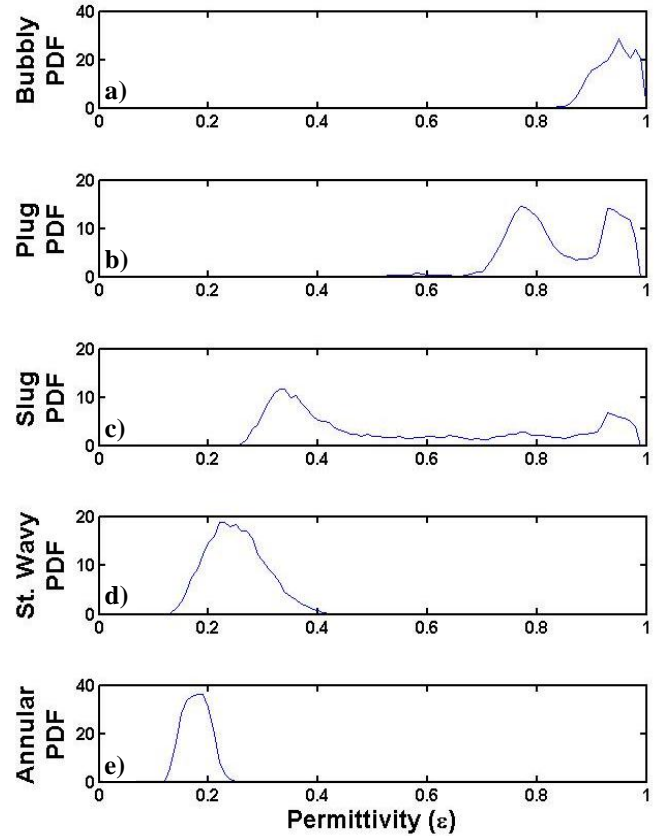
Figure 5. PDF of $\overline{\varepsilon^*}$ plotted for each flow regime: a) Bubbly, b) Plug, c) Slug, d) Stratified wavy, and e) Annular flows.

calculated by ECT Toolsuite. Each frame is spatially averaged resulting in a $\overline{\varepsilon^*}$ value. The averaged data results in a single column vector of $\overline{\varepsilon^*}$ data versus time, for each test point. Similar calculations form column vectors representing the minimum and maximum of each frame with respect to time.

To further reduce the data, several options are employed. Firstly, summary statistics of the $\overline{\varepsilon^*}$ data are calculated over the entire 256 frame data set (~15 seconds), including the mean, variance, skewness, and kurtosis. Using this data reduction technique reduces the number of data points by over 200,000 and formed four input parameters for each case. Unfortunately, this limited information proved insufficient to provide accurate flow regime identification.

Secondly, subsets of the data vector can be extracted to represent the entire signal. Obviously, care must be taken not to truncate too much data as important characteristics can be lost. Experience guides the decision between computational economy and data fidelity. The first 50 frames of each ECT data set were determined to capture the behavior while reducing the number of input data points.

Copyright © 2013 by ASME

Finally, the $\overline{\varepsilon}^*$ data can be represented by a PDF. The PDF is generated by applying a smoothed curve fit of $\overline{\varepsilon}^*$ histogram. A histogram partitions the data by counting the number of data points that fall within the boundaries of predetermined bins. In this way, the 256 length vector of $\overline{\varepsilon}^*$ data is summarized by N integer values, with N equal to the number of bins. The PDF provides a metric for observing the range and spread of the data. All data presented in this paper uses 50 bins to allow direct comparison with the inputs.

All three methods can be used independently or in combination to create input parameters for neural network training. Different combinations of concatenated data were used to provide training inputs. Four separate network inputs were used to test the performance for five flow regime labels. The first test used only the four summary statistics from 15 seconds of data. Second, fifty values of $\overline{\varepsilon}^*$ calculated from the first 50 frames of ECT data were used. Third, magnitudes of 50 PDF bins from three seconds of data were used. Finally, a combination of the four statistics, 50 values of $\overline{\varepsilon}^*$, and the 50 PDF bin magnitudes were used forming 104 inputs. The first and last networks from the five flow regime label tests can be directly compared with the results using seven flow regime labels.

Similar to the conclusions made by Rosa et al.[4] visual observations indicated that transition regions exhibited slightly different behavior and were therefore given different classification labels. However, closer examination after testing showed that the statistics and trends of $\overline{\varepsilon}^*$ values showed little difference. Reductions in the number of classifications from seven to five resulted in improved network accuracy during a second set of network training and testing.

Neural Network

An artificial neural network consists of an interconnected arrangement of computational nodes. Based on its arrangement, the neural network can map any number of inputs to any number of outputs. In our case, the number of outputs is one and consists of an integer regime classifier for each power and flowrate case. The various combinations of inputs to the neural network were described in the previous section.

For the current work, a function fitting neural network was employed with ten nodes in the hidden layer (see Figure 6). The nodes utilized a hyperbolic tangent transfer function. The input cases (ranging from 2-113 parameters for each of the 196 test points) were divided randomly such that 70% were used to train the neural network, 15% were used for validation, and 15% were used for testing. The training of the network was accomplished with the Levenberg-Marquardt algorithm and performance was tracked using the mean squared error[15]. The goal of training is to identify the constants that comprise the weights and biases of each artificial neuron.
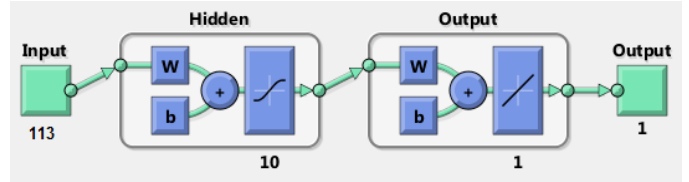

Figure 6. Schematic representation of present Neural Net architecture (generated by MATLAB).

A single training session does not produce a high correlation between the target regime classifiers and those predicted by the neural network. Consequently, the neural network is retrained by supplying it with newly randomized subsets of the input and target data. This is repeated until the neural network can predict the targets to a high accuracy, usually 90% or better. Since the outputs of the neural network are floating point numbers, they are rounded to the nearest integer before comparison to the target values. In the present work, the neural network had to be retrained around ten times to reach the desired accuracy.

Many different arrangements of the ECT data have been tried as inputs to the neural network with varying degrees of success. As mentioned before, the 104 length vector provided the best accuracy using five flow regime classifications. To evaluate a new case, an input vector was formulated from its raw data and sent to the neural network, which provided a single predicted value of flow regime.

RESULTS

The use of neural networks can be complicated by the plethora of options available, such as training methodology, number of nodes, number of hidden layers, error calculation, regularization method, and so forth. Adjustments were made to the training methodologies available in the software package. Ultimately, no method beyond the default one provided any better neural network performance or reduction in training time. Also, while heuristics exist to help guide one in choosing the number of layers and nodes, no more than the numbers presented earlier were required.

Figure 7 shows a map of the heater power and flowrate cases, separated into their visually determined flow regimes. Generally, there are demarcations between the regimes; however, overlapping data points do exist, especially along the boundaries. One reason for this is the often stochastic behavior of transition regimes, ones where the flow exhibits characteristics of two adjacent regimes. Great care has been taken to label these transitions correctly, or, in the case of great uncertainty, eliminate them altogether.

Figure 8 presents a smoothed PDF overlay showing all 196 cases on top of each other. This figure demonstrates that there is clear seperation between each of the first four flow regimes; however there is less of a distinction between stratified wavy and annular flows. Bubbly flow shows a single peak between permittivity vlaues of 0.8 and 1. Plug flow shows two peaks, one around 0.3 and a larger peak around 0.9. Slug flow similarly shows two peaks with the first occuring around 0.2

and the second occuring around 0.9. The difference between the two is the size and location of peaks. For plug flow the larger amplitude peak occurs at higher permittivity values indicating lower void fractions, while slug flow sees the larger peak at much lower permittivity values indicating higher void fractions. Another difference between these two flow regimes is the overall spread of the PDF. Slug flow typically has a wider range of permittivity values accounted for in each PDF curve, which is to be expected due to the larger difference between vapor and liquid levels. Stratified wavy flow has a single large peak occuring around 0.25 with a long tail on the right hand side. Ocassionally the tail ends with a peak around 0.9 indicating the occurance of short, large-ampltitude waves traveling through the channel. Finally, annular flow shows a single peak occuring for permittivity values between 0.1 and 0.2.
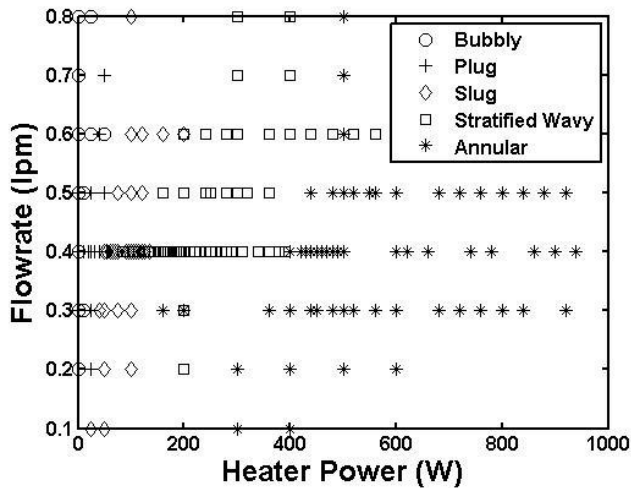
Figure 7. Flow map for the cases in the present work.

The largest possiblitiy of mislabled flow regimes occurs during the trasition regions between adjacent flow regimes. In this case, the flow is actually in one regime part of the time and the neighboring regime the rest and thus exibits characteristics of two flow regimes when averaged over a long enough time interval. Since the behaviour of stratified wavy closely resembles that of annular flow under certain circumstances, and flow velocities are much faster, a greater possiblility for mis-labeling occurs during this transition.

Table 2 presents the accuracy results from the neural networks using seven flow regime labels. The second column provides the number of cases tested for each flow regime listed in the first column. The third column presents the results of the percent accurate for each flow regime and an overall accuracy for the network generated using only the four summary statistics. This network identifies bubbly, plug and slug flow well, while performing poorly for elongated bubbly, intermittent, stratified wavy, and annular. Increasing the number of input parameters to include the four summary statistics, the 50 $\overline{\varepsilon}^*$ values, and the 50 bin PDF shows only a

slight improvement in overall accuracy with the most notable improvement occuring for annular flow.

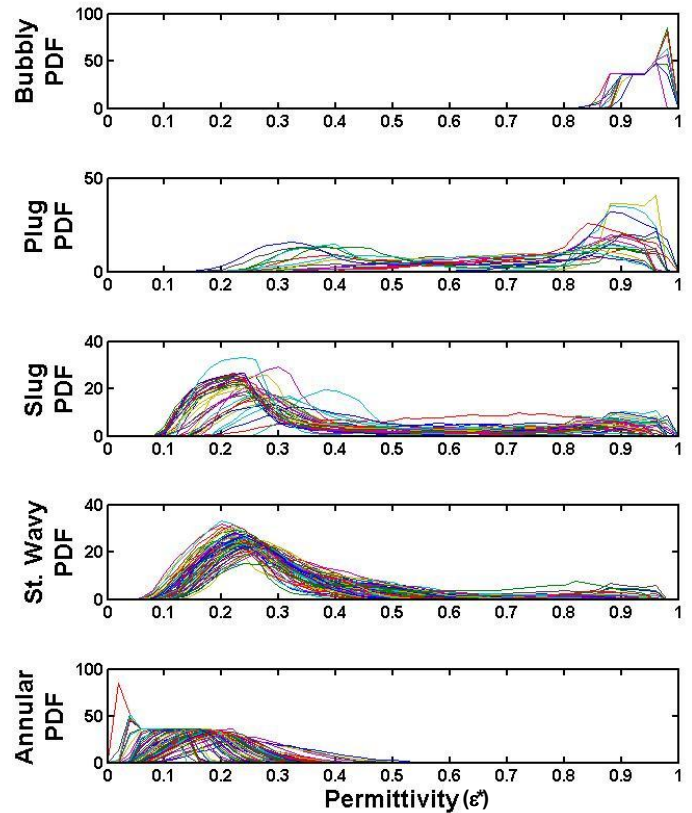**Figure 8.** Overlapping PDF plots for each flow regime show consistency in labeling for each of the five flow regimes.

Table 2. Seven-label flow regime identification results of neural network analysis for 196 test cases using a combination of statistics, $\overline{\varepsilon}^*$, and PDF values, forming 104 inputs.

Flow Regime	#	Stats (4)	Combined (104)
Bubbly	10	90.0	100
Elongated bubbly	2	50.0	100
Plug	18	94.4	88.9
Slug	35	91.4	82.9
Intermittent	65	72.3	75.3
St. Wavy	45	60.0	71.1
Annular	21	61.9	90.5
Total	**196**	**75%**	**80%**

Table 3 presents the neural network results for the five reduced flow regime classification labels. A second series of neural networks was created for four sets of input parameters. Similar to the data presented in Table 2 the first and second columns represent the flow regime labels and the number of test cases at each regime. The third column presents the accuracy for each regime using only the four summary statistics. Comparing the results in this column to the data presented using seven classifications shows a dramatic improvement from 75 % to 90 %. Next, the fourth and fifth columns show the results for the first 50 $\overline{\varepsilon}^*$ values and 50 PDF

bins respectively. Each of these methods alone shows a further increase to 97% with a couple regimes seeing 100 % accuracy for each. Finally, the last column presents the concatenation of summary statistics, 50 $\bar{\varepsilon}^*$ and 50 PDF bins. As would be expected this results in better agreement and the network shows almost perfect accuracy of 99%.

Table 3. Five-label flow regime identification results of four separate neural networks, comparing statistics, $\bar{\varepsilon}^*$, PDF, and a combination of all three (Number of input parameters in parenthesis).

Flow Regime	#	Stats (4)	ECT (50)	PDF (50)	Combined (104)
Bubbly	12	100	100	100	100
Plug	18	83.3	83.3	100	100
Slug	35	91.4	97.1	91.4	94.2
St. Wavy	65	81.5	96.9	98.5	100
Annular	66	96.7	100	96.7	100
Total	**196**	**90%**	**97%**	**97%**	**99%**

Figure 9 presents error histograms for the combined input values for seven and five classification labels respectively. Using unrounded output values generated from the trained neural network and taking the difference with the expected target values provides a value that tracks how far off the network was with each prediction. Since the network generates output values on either side of the expected target the histogram shows both positive and negative values showing both over and under predictions. Any error value within ± 0.5 will represent correct regime identification. Any value outside of these bounds is considered to be incorrect. Values ranging between 0.5 and 1.5 on either side will represent a misclassification by one regime. Values larger than this are off by more than one regime. It is clear from Figure 9 that reducing the number of flow regime classifications from seven to five results in much less error, with no errors larger than 1.5 indicating that all data is within one flow regime of the expected targets.

Accuracy of the neural networks improved from 80% to 99% by reducing the number of flow regime classifications from seven to five. This improvement shows that transition cases exhibiting behavior of adjacent flow regimes prove difficult for neural networks to identify. Further testing is recommended to analyze this dependency in more detail.
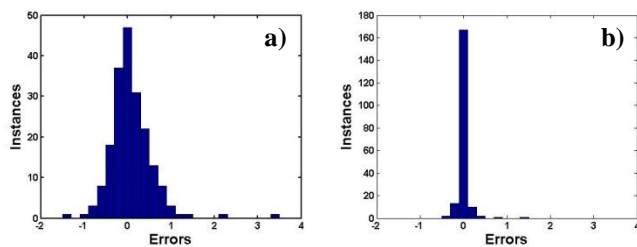

Figure 9. Histogram of errors for the combined data, comparing: a) 7 classification labels to b) 5 classification labels.

CONCLUSION

A novel technique for automated flow regime identification was presented in this paper. ECT signals were tracked for 196 different test points by adjusting flow rate and heater input power for horizontal 7mm channel flows of R134a. Mean normalized permittivity ratio values studied over time were compared to visual analysis of high speed videos using a neural network.

The results presented in this paper clearly show that using the five most commonly documented flow regime classification labels in the literature resulted in better performance by the neural network. An 80% accuracy was seen using seven flow regime labels and 104 input parameters combining the four summary statistics, 50 ECT values, and 50 PDF bins. Reducing the number of flow classifications to five and only using the four summary statistics resulted in an improvement to 90%. Additional improvements from 90% to 99% were realized by increasing the number of input parameters from four to 104 by combining a three input types.

Limitations of the currently developed neural network were test points that exhibited behavior of two separate flow regimes. Transition points need to be investigated further by the use of two and three level neural networks. Additionally desired tests include a comparison of the neural network developed for this paper with a new channel setup using different size channels.

ACKNOWLEDGMENTS

REFERENCES

[1]Thome, J. R., "State-of-the-Art Overview of Boiling and Two-Phase Flows in Microchannels," *Heat Transfer Engineering*, Vol. 27, No. 9, 2006, pp. 4-19.

[2]Kandlikar, S. G., "Heat Transfer Mechanisms During Flow Boiling in Microchannels," *Journal of Heat Transfer*, Vol. 126, No. 1, 2004, pp. 8-16.

[3]Kreitzer, P. J., Byrd, L., and Willebrand, B. J., "Initial Investigation of Two Phase Flow Characterization of R134a in a Horizontal Channel using High Speed Video Analysis and Electrical Capacitance Tomography," *42nd AIAA Thermophysics Conference*. Hawaii, 2011.

[4]Rosa, E. S., Salgado, R. M., Ohishi, T., and Mastelari, N., "Performance comparison of artificial neural networks and expert systems applied to flow pattern identification in vertical ascendant gas–liquid flows," *International Journal of Multiphase Flow*, Vol. 36, No. 9, 2010, pp. 738-754.

[5]Elperin, T., and Klochko, M., "Flow Regime Identification in a Two-phase Flow using Wavelet Transform," *Experiments in Fluids*, Vol. 32, 2002, pp. 674-682.

[6]Brutin, D., Topin, F., and Tadrist, L., "Experimental Study of Unsteady Convective Boiling in Heated Minichannels,"

International Journal of Heat and Mass Transfer, Vol. 46, No. 16, 2003, pp. 2957-2965.

[7]Tran, T. N., Chyu, M. C., Wambsganss, M. W., and France, D. M., "Two-Phase Pressure Drop of Refrigerants During Flow Boiling in Small Channels: an Experimental Investigation and Correlation Development," *International Journal of Multiphase Flow*, Vol. 26, No. 11, 2000, pp. 1739-1754.

[8]Halow, J. S., and Nicoletti, P., "Observations of Fluidized Bed oalescence Using Capacitance Imaging," *Powder Technology*, Vol. 69, No. 3, 1992, pp. 255-277.

[9]Loser, T., Wajman, R., and Mewes, D., "Electrical Capacitance Tomography: Image Reconstruction Along Electrical Field Lines," *Measurement Science and Technology*, Vol. 12, No. 8, 2001, pp. 1083-1091.

[10]Hu, H. L., Dong, J., Zhang, J., Cheng, Y. J., and Xu, T. M., "Identification of gas/solid two-phase flow regimes using electrostatic sensors and neural-network techniques," *Flow Measurement and Instrumentation*, Vol. 22, No. 5, 2011, pp. 482-487.

[11]Mi, Y., Ishii, M., and Tsoukalas, L. H., "Flow regime identification methodology with neural networks and two-phase flow models," *Nuclear Engineering and Design*, Vol. 204, No. 1–3, 2001, pp. 87-100.

[12]Mishima, K., and Ishii, M., "Flow Regime Transition Criteria for Upward Two-phase Flow in Vertical Tubes," *International Journal of Heat and Mass Transfer*, Vol. 27, 1983, pp. 723-737.

[13]Ghosh, S., Pratihar, D. K., Maiti, B., and Das, P. K., "Identification of flow regimes using conductivity probe signals and neural networks for counter-current gas–liquid two-phase flow," *Chemical Engineering Science*, Vol. 84, No. 0, 2012, pp. 417-436.

[14]Kreitzer, P. J., Hanchak, M., and Byrd, L., "Horizontal Two Phase Flow Regime Identification: Comparison of Pressure Signature, Electrical Capacitance Tomography (ECT) and High Speed Visualization," *International Mechanical Engineering Congress & Exposition*. ASME, Houston, TX, 2012.

[15]TheMathWorks, "MATLAB." Natick, MA, R2011a.